



## Effect of Tubular Solar Absorber on Performance of Counterflow Double Pass Solar Air Heater: Experimental and Numerical Studies

N. F. Hussein<sup>\*a</sup>, S. T. Ahmed<sup>b</sup>, A. L. Ekaid<sup>a</sup>

<sup>a</sup> University of Technology, Baghdad, Iraq.

<sup>b</sup> Bilad Alrafidain University College, Diyala, Iraq

### PAPER INFO

### ABSTRACT

#### Paper history:

Received 09 June 2022

Received in revised form 06 July 2022

Accepted 10 July 2022

#### Keywords:

Solar Air Heaters

Thermal Storage

Double Pass

Thermos-hydraulic Efficiency

Tubular Capsules

The problem of solar radiation intermittency can significantly affect the thermal performance of solar air heaters (SAHs). The efficient solution for this problem is utilizing thermal storage to store the thermal energy and using it again in off sunshine hours. The present study analyzed the thermal performance of two configurations of counterflow double pass solar air heater. The first configuration included a conventional flat plate solar absorber, while the second configuration involved tubular capsules that are filled with water as a sensible thermal storage material. The tubular capsules have been installed longitudinally in parallel to the direction of airflow. The study involved numerical and experimental parts. The results showed a remarkable enhancement in useful energy production when using the tubular capsules. Moreover, the SAH with tubular capsules can produce useful energy for a longer time due to the presence of the thermal storage material within capsules. It is found that the total useful energy in the case of tubular capsules is about 4082, 4295.3, 4426, 4584, and 4693 W at a mass flow rate of 0.03, 0.025, 0.02, 0.015, and 0.01 kg/s, respectively, with an increment of 39.1, 51.2, 59.4, 74.8, and 89.6%, respectively as compared with the flat-plate absorber. In addition, the average thermo-hydraulic efficiency in the case of tubular capsules are higher than those values which are achieved in flat plate case by about 9.3, 15, 19.6, 28.2, and 40% at a mass flow rate of 0.03, 0.025, 0.02, 0.015, and 0.01 kg/s, respectively.

doi: 10.5829/ije.2022.35.10a.18

### NOMENCLATURE

$A_c$	Collector area ( $\text{m}^2$ )	$T_{air,out}$	Outlet air temperature ( $^{\circ}\text{C}$ )
$Cp_{air}$	Specific energy of air ( $\text{J}/\text{kg}^{\circ}\text{K}$ )	$T_{air,in}$	Inlet air temperature ( $^{\circ}\text{C}$ )
$Cp_w$	Specific energy of water ( $\text{J}/\text{kg}^{\circ}\text{K}$ )	$\Delta T_{Tw2-Tw1}$	Water temperature rise ( $^{\circ}\text{C}$ )
$I$	Solar radiation ( $\text{W}/\text{m}^2$ )	$t$	Time period between two measurements (s)
$m_{air}$	Air mass flow rate ( $\text{kg}/\text{s}$ )	$\eta_{th,charge}$	Thermal efficiency in charge period.
$m_w$	Water mass (kg)	$\eta_{th,discharge}$	Thermal efficiency in discharge period.
$Q_{in}$	Received energy (W)	$\eta_{eff,charge}$	Thermo-hydraulic efficiency in charge period
$Q_{mechanical}$	Pumping power (W)	$\eta_{eff,discharge}$	Thermo-hydraulic efficiency in charge period
$Q_{useful}$	Useful energy gain (W)	$P$	Pressure drop (Pa)
$Q_s$	Stored energy (W)	$\rho_{air}$	Air density ( $\text{kg}/\text{m}^3$ )
$T_{air,in}$	Inlet air temperature ( $^{\circ}\text{C}$ )		

### 1. INTRODUCTION

Conventional energy sources such as fossil fuels are limited and affected by supply problems and unstable

prices [1]. Moreover, burning fossil fuels produce harmful emissions that are associated with many respiratory diseases and are responsible for environmental pollution and global warming [2]. These

\*Corresponding Author Institutional Email:  
[50153@uotechnology.edu.iq](mailto:50153@uotechnology.edu.iq) (N. F. Hussein)

serious problems and challenges pushed the world to invest effectively in other alternative sources such as renewable energies. Solar energy is a promising source of unlimited and clean energy. Solar energy can be invested directly either in electrical energy generation by using photovoltaic systems [3] or in thermal energy generation by utilizing various systems for instance solar air dryers [4], solar water collectors [5], solar towers [6], solar chimneys [7], etc. Solar air heaters are simple in their design and installation. The conventional solar air heaters consist of a transparent cover which is usually made from glass material to minimize the top heat losses to the surroundings [8], solar absorber plate that is usually made from metal to absorb solar energy in thermal energy form, air channels, an electric air blower to supply air to the system, and thermal insulation to reduce thermal losses from back and sides of the collector [9]. Solar air heaters are utilized in many applications that work under low or mild temperatures [10], for instance drying textile, agricultural, and marine products, in addition to dehumidifying and heating the interiors of buildings to create a comfortable environment, especially in the winter season or in cold zones [11]. However, solar air heaters suffer from some drawbacks represented by energy losses, a low thermal performance due to the low convective heat transfer coefficient between the airflow and the surface of the solar absorber plate, and the solar intermittency problem that make the conventional solar air heaters cannot meet the application's requirements after the sunset or during off-sunshine hours [12]. Research is continuously conducted to find the best solutions for these drawbacks. Regarding reducing the lost energy, Kumar and Subhash [13] studied the effect of glass cover number, and they concluded that increasing the cover layers can reduce the top heat loss, but at the expense of the amount of solar radiation reaching the absorbing surface, Kumar et al. [14] used a number of low-cost thermal insulating materials (bubble wrap and ceramic wool) and tested their influence on the collector's performance. They revealed that using ceramic wool can reduce the thermal losses from the collector's body and rise the thermal efficiency by approximately 5.6%. Abdelkader et al. [15] studied the effect of painting the solar absorber plates with paints based on nanoparticles technology. The researchers showed that mixing nanoparticles with paint led to an increase in the outlet air temperature by approximately 20% because of enhancing the optical characteristics of paint. On the other hand, many researchers focused on solving the problem of low convective heat transfer coefficient by adopting various techniques. For example, Das et al. [16] enhanced the convective heat transfer coefficient by up to 17% by creating artificial roughness by mixing the sand particles with the black paint. Jalil et al. [17] tested the effect of installing wavy fins of 3 and 7 waves on the solar flat plate absorber, and they

succeeded in improving the thermal performance by about 84% as compared with the conventional collector. Sudhakar and Cheralathan [18] improved the thermal performance by up to 17.4% by replacing the conventional flat plate absorber with V-groove absorber with pin fins on its two sides. Mesgarpour [19] studied numerically enhancing the thermal performance by creating a helical flow path by replacing the conventional flat plate absorber with helical channels. The results showed that these helical channels increased the heat transfer area up to 24.18%, hence, enhancing thermal performance. In addition, a new technology that involved replacing conventional flat plate absorbers with novel configurations that can be filled with thermal storage materials was adopted by many researchers to solve the problem of solar energy intermittency. Jalil and Ali [20] studied the effect of adding steel wool as a sensible thermal storage material in the lower channel of the collector. The thermal performance is enhanced by about 79.82% when using steel wool at a porosity of 0.9625.

Sajawal et al. [21] replaced the conventional flat-plate absorber with finned tubes filled with phase change material (RT44HC and RT18HC). The study outcomes revealed that the thermal performance rise to 71.6% by using a mixture of (RT44HC and RT18HC) instead of using them separately. Muthukumaran and Senthil [22] tested new designs of solar absorbers which are straight tubes and spiral coiled that are filled with a mixture of paraffin wax and glycerol. The results showed that the spiral coiled absorber offered superior thermal performance than the straight tubes and the conventional flat plate absorbers. Moreover, integrating thermal storage with the solar collector can stores thermal energy for a short time during off-sunshine hours or after sunset, hence enhancing the uniformity of outlet air temperature. Raju and Kumar [23], Sudhakar and Cheralathan [24] adopted encapsulated phase change material technology to improve thermal performance. Using this technique can enhance thermal efficiency in the range of 9-15%. Abed [25] used a mixture of paraffin wax and sand as new thermal storage material, different mixing ratios have been tested, and the outcomes revealed that mixing 20% of paraffin wax with sand raise the air temperature rise up to 9.2% and gives the best thermal performance. Using built-in thermal storage technology within the double-pass solar air heaters is still under development and requires more research. Moreover, the three-dimensional mathematical models that adopt finite volume schemes and are related to forced convection turbulent flow inside a counterflow double-pass solar air heater with built-in thermal storage are very few. Therefore, this study offers a new design of the solar absorber within the counterflow double-pass solar air heater that is tubular capsules filled with a sensible thermal storage material.

## 2. NUMERICAL METHOD

### 2. 1. Geometry

The two configurations are created by using CFD software ANSYS Fluent version (2021 R2). The geometry of the two configurations is performed by a designed modeler of the ANSYS workbench. Generally, the two configurations included glass cover, solar absorber (flat plate for the first configuration and tubular capsules for the second configuration), backplate, and thermal insulation. The generated configurations are presented in Figure 1.

### 2. 2. Meshing

The meshing process for the two configurations was performed by using the meshing tool in the ANSYS workbench (2021 R2) as shown in Figure 2. Structured mesh with mesh element size equal to 1365379 has been generated, and the dependency of mesh on the solution's accuracy was achieved by doing an independent mesh test, where the mesh concentration is gradually increased until the variation in outlet temperature becomes less than 1% as shown in Figure 3.

### 2. 3. Assumptions

The case is assumed three-dimensional (3D), and the airflow through the upper and lower channels is assumed forced convection turbulent incompressible flow. In addition, the thermophysical characteristics of the airflow are assumed constant. The fluid inside the tubular capsules is selected liquid water. The solar rate is assumed uniform and equals  $1000 \text{ W/m}^2$ , and the inlet thermal condition equals  $25^\circ\text{C}$ . Moreover, both the back and side walls of the collector are assumed insulated.

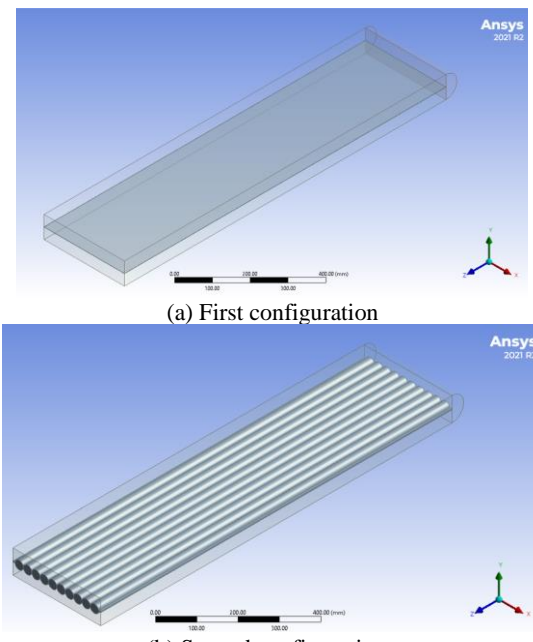


**Figure 1.** The geometry of the configurations

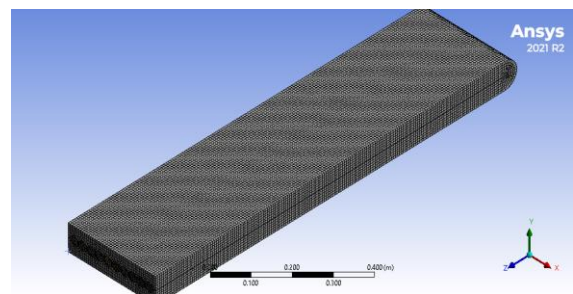


**Figure 2.** Meshing configurations

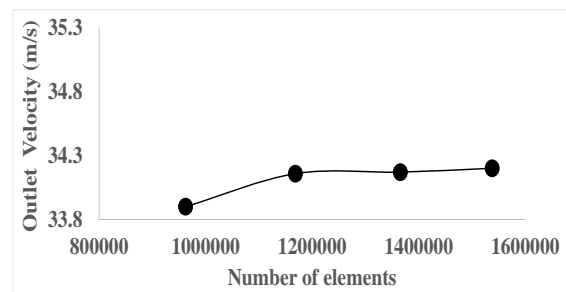


**Figure 3.** Mesh independence test's outcomes

### 2. 4. Boundary Conditions and Operating Parameters

The operating parameters and boundary conditions that are applied in the simulation are listed in Table 1. In addition, the properties of both glass cover, backplate, and tubular capsules are listed in Table 2.

### 2. 5. Solution Method

The finite-volume method with a semi-implicit pressure-linked algorithm (SIMPLE) has been used to solve the governing equations. In addition, a second-order upwind scheme is

**TABLE 1.** Operating parameters and boundary conditions

Boundary condition	Value
Solar rate	$1000 \text{ W/m}^2$
Mass flow rate	0.01, 0.015, 0.02, 0.025 and 0.03 kg/s.
Inlet air temperature	$25^\circ\text{C}$
Wind velocity	1 m/s

**TABLE 2.** Properties of the glass cover, backplate, and absorber.

Property	Glass cover	Backplate	Absorber
Thermal conductivity (W/m.K)	1.4	80	387.6
Specific heat (J/kg.K)	770	450	381
Density (kg/m <sup>3</sup> )	2540.4	8013	8978

applied for discretizing the governing equations. The renormalization group (RNG)-  $k-\varepsilon$  model which is the most common model for describing turbulent flow behaviors. Kumar et al. [26] have chosen for simulating turbulent flow as well as heat transfer since this model gives approximately the same results as both the Blasius empirical correlation and the Dittus-Boelter empirical correlation [27]. The convergence criteria for continuity, momentum, and energy equations are set to 1e-03, 1e-03, and 1e-06, respectively.

### 3. EXPERIMENTAL SETUP

**3.1. General Description** The main components of the experimental setup as shown schematically in Figure 4 are a counterflow double pass solar air heater (CFDPSAH), an artificial solar simulator, an electrical air blower, U-tube manometer, orifice meter, thermocouples, and a data logger.

The body of the solar air heater is constructed as a rectangular box from a 1.8 cm thick plywood sheet. The collector body is divided into upper and lower channels which are separated by a solar absorber. The collector's projected area is  $1200 \times 300$  mm. The upper channel is covered by a glass cover with a thickness of 4 mm and a transmittance of 88% for the purpose of allowing maximum solar radiation rate to fall on the solar absorber and preventing long-wave radiation to escape to the surrounding. The galvanized plate of 1 mm thick has been placed in the lower channel to invest some of the thermal losses. Two configurations of solar absorber as shown in Figure 5 have been used, the first configuration is a flat plat absorber as a reference, and the second configuration is a set of tubular capsules which are fitted in parallel to the direction of airflow.

The upper side of solar absorbers is coated with black paint to enhance the absorptivity of absorbers for solar radiation. The tubular capsules have been filled with a

sensible thermal storage medium (water). An electrical air blower is utilized to supply air to the solar air heater, and a manual valve which is attached to the pump side of the air blower is used to adjust the air mass flow rate. Different mass flow rates (0.01–0.03 kg/s) with increment of 0.005 are adopted in experiments. The artificial solar radiation rate (average value equal to  $1000 \text{ W/m}^2$ ) is achieved by using an artificial solar simulator which is controlled by utilizing variac transformation. The pressure difference through the solar heater is measured by connecting the measuring device to two tapes which are fixed at the inlet and outlet of the solar heater. Thirty-eight thermocouples (type K) were used to monitor the temperature distribution in the solar heater during the experiment time. These thermocouples were installed in different locations which are: four thermocouples were fitted in each of glass cover, the middle height of the upper and lower channels, the upper and lower side of the solar absorber, and the upper side of the backplate, as well as twelve thermocouples inside the tubular capsule. Moreover, two thermocouples were mounted at the inlet and outlet of the solar heater. The positions of measuring points are shown in Figure 6. The dimensions and specifications of solar air heater configurations as well as the details of the materials that are used in the experimental setup are listed in Table 3.



Figure 5. Solar absorber configurations

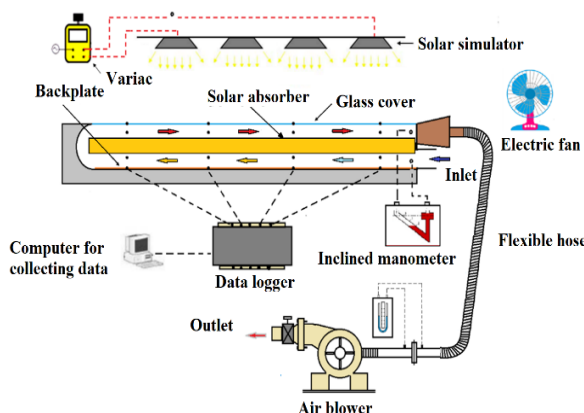


Figure 4. Schematic of the experimental setup

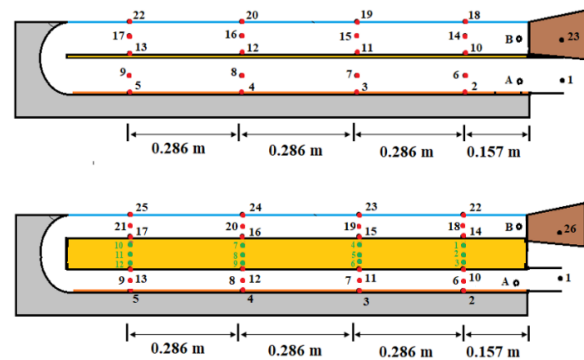


Figure 6. Measuring points locations

**TABLE 3.** Dimensions and specifications of solar air heater configurations

Item	Details
Double pass solar air heater	
Total length	1260 mm
Total width	340 mm
Total height	80.9 mm
Effective length	1200 mm
Effective width	300 mm
First absorber configuration (copper flat plate)	
Height of upper & lower channels	40 mm
Plate thickness	0.9 mm
Plate length	1200 mm
Plate width	30 mm
Second absorber configuration (copper tubular capsules)	
Height of upper & lower channels	32.15 mm
Length	1200 mm
Outer Diameter	28.6 mm
Inner Diameter	26.7 mm
Thickness	0.9 mm
Number of capsules	10
Insulation (Polyurethane foam)	
Thickness	50 mm
Absorber coating (black paint Rust-oleum)	
Absorptivity	92%

**3.2. Instruments and Measuring Devices** The details and specifications of instruments and measuring devices that are used in experiments are summarized in Table 4.

**TABLE 4.** Details and specifications of instruments and measuring devices

Instrument type	Model	Purpose of usage	Accuracy level
Solar power meter	SPM-1116SD	Measuring solar intensity	$\pm 5\%$
Orifice meter + U tube manometer	-	Measuring mass flow rate	$\pm 5\%$
Data logger	AT-4524	Measuring temperatures	$\pm 0.8^\circ\text{C}$
Digital Thermometer	HT-9815	Measuring temperatures	$\pm 2^\circ\text{C}$
Inclined manometer	-	Measuring pressure drop	$\pm 2\%$

### 3.3. Experimental Procedure and Data Analysis

#### 3.3.1. Experimental Procedure

The temperature of all thermocouples at the beginning of the experiment should be equal to  $25^\circ\text{C}$  which is the same temperature as the room. After that, the electric air blower and the artificial solar simulator are switched on at the desired value. Then, the system is kept running until the system reaches a steady-state, and during this time, the readings of all thermocouples are measured every 5 minutes. Finally, when the steady-state is achieved at the end of the charge period after 1 hour, all temperatures and the pressure drop across the solar air heater are recorded. After that, the solar simulator is switched off and the discharge period starts. During the discharge period, measuring of all temperatures continues. The discharge period ends when the temperature difference between the inlet and the outlet equals approximately zero.

#### 3.3.2. Data Analysis

Depending on the first law of thermodynamics, the solar air heater's performance can be evaluated by the following formulas [28, 29]:

$$\eta_{th,charging} = \frac{Q_{useful}+Q_s}{Q_{in}} \quad (1)$$

$$\eta_{th,discharging} = \frac{Q_{useful}}{Q_s} \quad (2)$$

where  $Q_{useful}$ ,  $Q_{in}$ , and  $Q_s$  represent the useful energy gained from solar air heater, received energy from solar source and stored energy which can be represented by the following formulas:

$$Q_{useful} = m_{air} \cdot Cp_{air} (T_{air,out} - T_{air,in}) \quad (3)$$

$$Q_{in} = A_c \cdot I \quad (4)$$

$$Q_s = m_w \cdot Cp_w (T_{w,2} - T_{w,1})/t \quad (5)$$

For the first configuration, the stored energy ( $Q_s$ ) is assumed zero due to the absence of thermal storage material. The term thermo-hydraulic efficiency or effective efficiency is used to take into account the influence of pressure drop on the solar air heater performance which can be calculated as follows [30]:

$$\eta_{eff,charge} = \frac{Q_{useful}+Q_s-Q_{mechanical}}{Q_{in}} \quad (6)$$

$$\eta_{eff,discharge} = \frac{Q_{useful}-Q_{mechanical}}{Q_s} \quad (7)$$

$$Q_{mechanical} = \frac{m_{air} \times \Delta p}{\rho_{air}} \quad (8)$$

where  $Q_{mechanical}$  is the needed pumping power for supplying air through the system.

## 4. RESULTS AND DISCUSSION

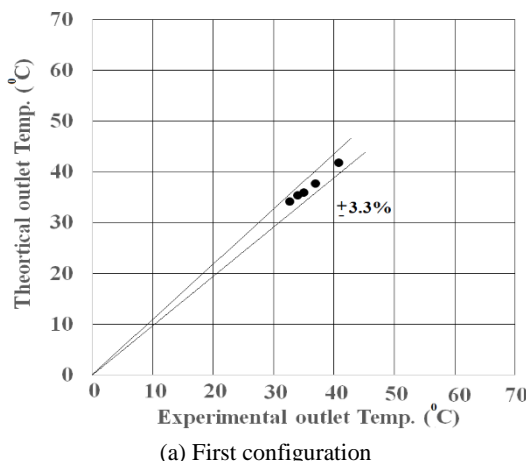
The numerical and experimental outcomes show the effect of replacing the conventional flat plate absorber with the tubular capsules on the thermal performance of the solar air heater. The validation between the numerical and experimental results has been made. In addition to that, a comparison between the conventional and proposed absorber in terms of total useful power and average thermo-hydraulic efficiency is presented.

**4. 1. Validation between Experimental and Numerical Work** The validation between experimental and numerical work is carried out, and the result is presented in Figures 7(a) and 7(b). The deviation within the acceptable agreement in ranges between 4% to 8.2 %.

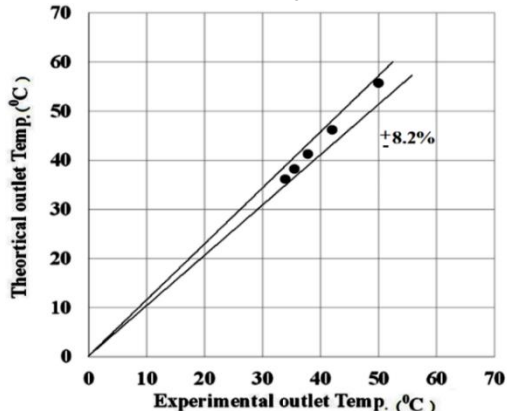
### 4. 2. Experimental Results

**4. 2. 1. Temperature Distribution** The principal purpose of SAHs is supplying hot air to use it in housings heating, industrial applications, etc. The

assessment of the temperature distribution of outlet airflow for the two configurations at different mass flow rates is shown in Figure 8. The results indicate that the outlet air temperature in the first configuration is greater than those temperature values in the second configuration, and this result can be attributed to saving part of absorbed solar energy by the absorber in the thermal storage material, in addition to decreasing the reflected solar radiation from the absorber through the glass cover to the surrounding (top heat loss) due to the special design of tubular capsules that causes internal reflections between the curvature surfaces of the absorber [31]. However, it can be noted that the second configuration can produce hot air for a longer time due to the presence of thermal storage material inside the tubular capsules which acts as an energy source that supply the airflow by energy during the discharge period. In addition, it can be seen from these figures that the outlet temperature also decreases with rising air mass flowrate due to increasing the convection process. It is found that at the end of the charge period, the outlet air temperature at a mass flow rate of 0.03 kg/s for second and first configurations is 32.7 °C, and 33.9 °C, respectively, and these temperatures increased by 24.7%, and 47% at 0.01 kg/s to become 40.7 °C, and 50 °C,

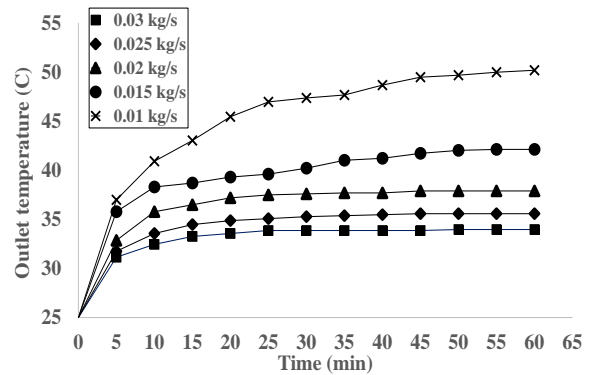


(a) First configuration

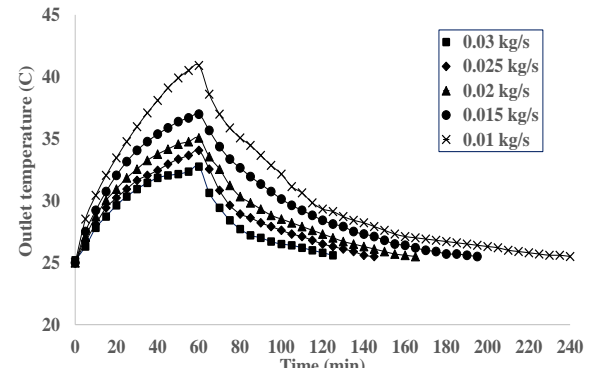


(b) Second configuration

**Figure 7.** Validation between experimental and numerical work



(a) First configuration



(b) Second configuration

**Figure 8.** Temperature distributions

respectively. Hence, this means that the percentage of rising outlet air temperature increases with decreasing the mass flow rate due to an increase in heat transfer rates from the absorber to airflow [32].

#### 4. 2. 2. Total Useful Energy

The total useful energy represents an important parameter in calculating the thermal performance of a solar air heater. Figure 9 displays the total values of the useful energy that is extracted from the solar absorber via the airflow at different mass flow rates. It can be seen from this figure that there is a significant increase in useful energy production when using the tubular capsules. It is found that the second configuration produces total useful energy of about 4082, 4295.3, 4426, 4584, and 4693 W at a mass flow rate of 0.03, 0.025, 0.02, 0.015, and 0.01 kg/s, respectively. The findings also show that the total useful energy that is extracted by the second configuration is significantly higher than the extracted useful energy in the first configuration by about 89.6, 74.8, 59.4, 51.2, and 39.1% for mass flow rates of 0.01, 0.015, 0.02, 0.025, and 0.03, respectively. This can be attributed to accumulated energy in the thermal storage medium which is invested in the discharge period.

#### 4. 2. 3. Average Thermo-hydraulic Efficiency

The thermo-hydraulic efficiency is a general parameter that is used not only for evaluating the SAHs performance but also for indicating the future research enhancement of SAHs performance. The assessment of the average thermo-hydraulic efficiency of both first and second configurations at various mass flow rates is stated in Figure 10. This figure reveals that the average thermo-hydraulic efficiency in the second configuration increases despite the decrease in mass flow rate values. This result can be attributed to the presence of thermal storage material (water) inside the proposed absorber that in turn feeds the airflow by the thermal energy during the discharge period, and this discharge period increases

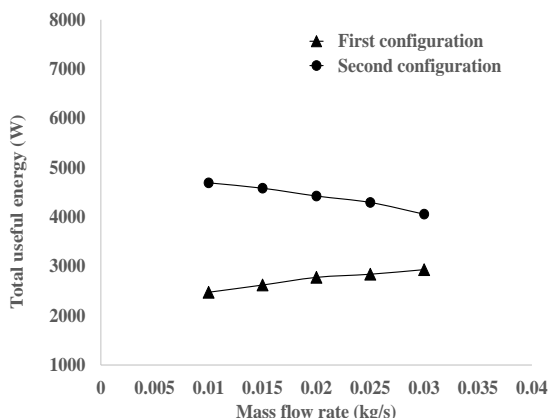


**Figure 9.** Total useful energy

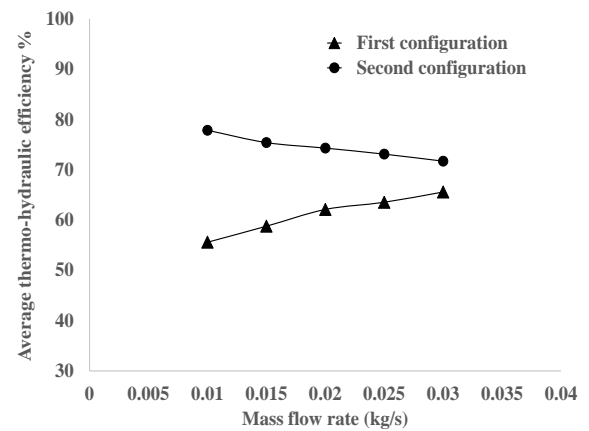


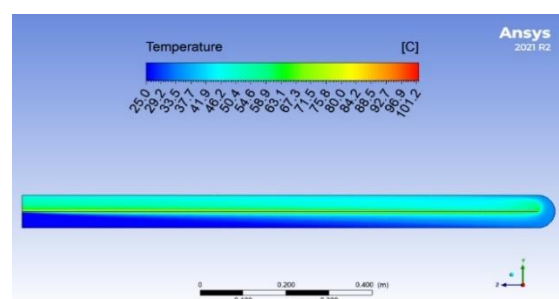
**Figure 10.** Average thermo-hydraulic efficiency

more and more as the air mass flow rate decreases, hence, producing useful energy for a longer time. Moreover, it is found that the average thermo-hydraulic efficiency for the second configuration is higher than the efficiency values of the first configuration because of the extra energy that is supplied to airflow in the discharge period which is not available in the first configuration case. The average thermo-hydraulic efficiency of the second configuration is about 71.7, 73.1, 74.3, 75.4, and 77.85% at air mass flow rates of 0.03 kg/s, 0.025 kg/s, 0.02 kg/s, 0.015 kg/s, and 0.01 kg/s, respectively, with increment of about 9.3, 15, 19.6, 28.2, and 40% at a mass flow rate of 0.03, 0.025, 0.02, 0.015, and 0.01 kg/s, respectively as compared with first configuration.

### 4. 3. Numerical Results

#### 4. 3. 1. Temperature Distribution Contours

The temperature distribution of airflow at a minimum and maximum flow rates for the two configurations is presented in Figures 11(a)-11(d). It can be observed that the temperature of airflow increases as the air moves forwards through the path of the collector's channels, and this increase in airflow temperature can be attributed to the stored thermal energy in the solar absorber, which in turn transfers to the airflow when it passes over the absorber surfaces. In addition, the outlet air temperature



(a) (First configuration),  $m=0.01 \text{ kg/s}$

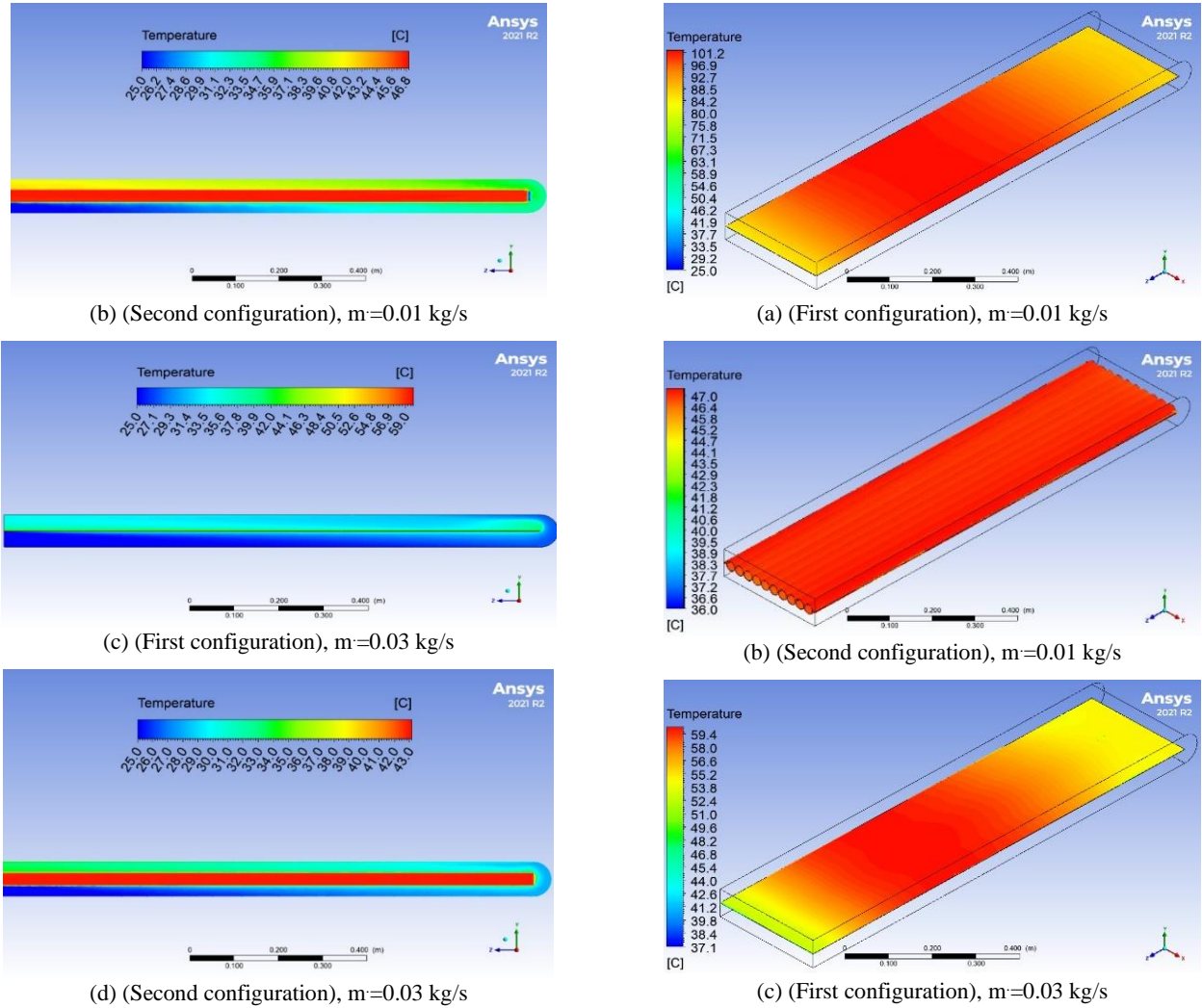


**Figure 11.** Temperature distribution of airflow

decreases as the mass flow rate increases because the convection exchange decreases as the airflow speed increases [33]. Furthermore, it can be noted that the airflow temperature in the second configuration is less than the airflow temperature in the first configuration because part of the absorbed energy is stored in the thermal storage material.

Figures 12(a)-12(d) show the temperature distribution of the absorber for the two configurations at the end of the charge period. It can be observed that the temperature distribution increases towards the middle point of the solar collector and decreases beyond this point to the end of the collector, and this result may be attributed to the role of vortices that are created at the start zone of the upper channel which in turn cause mixing up the airflow, hence, rising heat transfer rate between the absorber and the airflow [34]. Moreover, these figures indicate to the inverse relationship between airflow rate and absorber temperature.

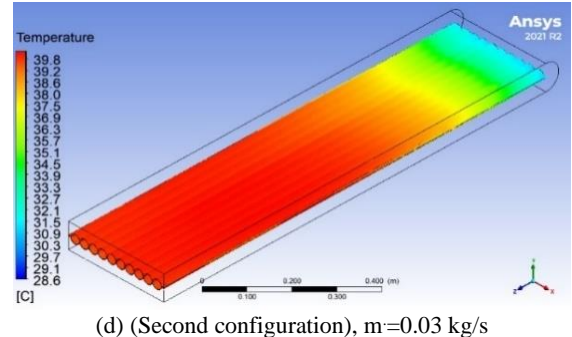


**Figure 12.** Temperature distribution of solar absorber configurations

#### 4.3.2. Air Velocity Vectors

Figures 13(a)-13(d) describe the velocity vectors at minimum and maximum mass flow rates for the two configurations. The maximum velocity is located at the end of the lower channel, and the flow separation occurs at the beginning of the upper channel. Moreover, the flow separation increases as the air mass flow rate increases.

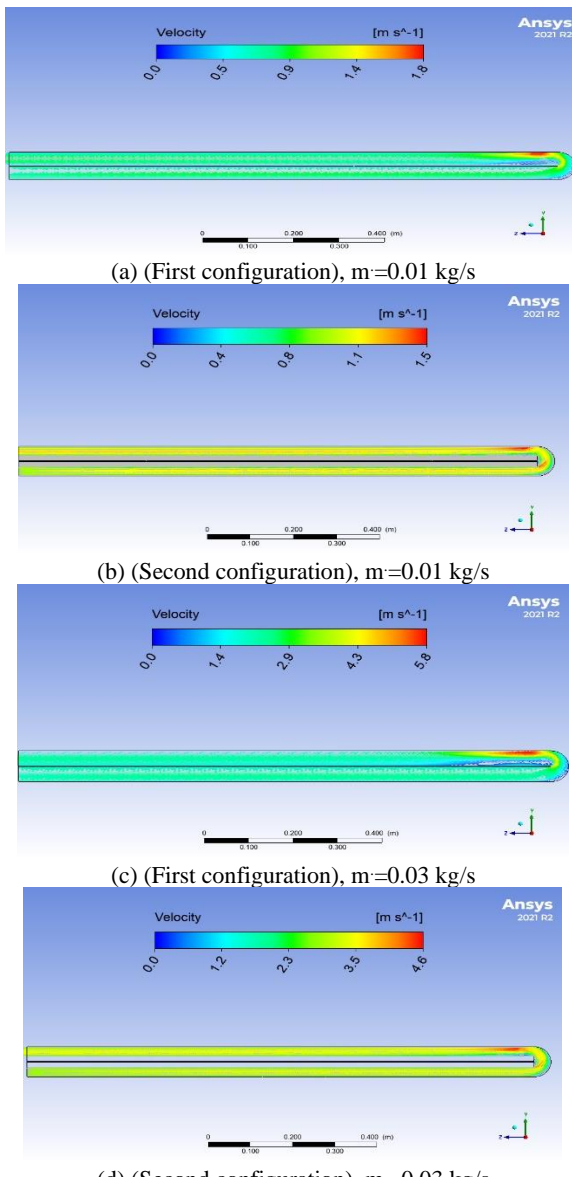


**Figure 13.** Velocity vectors of airflow

## 5. CONCLUSIONS

The outcomes of the present work can be summarized in the following brief points:

1. the second configuration can supply useful power for a longer time as compared with the first configuration due to the presence of thermal storage material.
2. The total useful energy generated by the second configuration is greater than those values that are achieved by the first configuration by an increment of 39.1, 51.2, 59.4, 74.8, and 89.6% at mass flow rates of 0.03, 0.025, 0.02, 0.015, and 0.01, respectively.
3. The second configuration offers higher average thermal performance compared to the first configuration

with an increment of about 9.3, 15, 19.6, 28.2, and 40% at a mass flow rate of 0.03, 0.025, 0.02, 0.015, and 0.01 kg/s, respectively.

4. Depending upon the findings of this work, it can be claimed that the feasibility of using the tubular capsules solar absorber as a thermal performance enhancer.

## 6. ACKNOWLEDGMENT

The authors are thankful to the University of Technology- Iraq for providing help in completing this work.

## 7. REFERENCES

1. Chaichan, M.T., Abass, K.I. and Kazem, H.A., "The impact of thermal storage materials on the heating and storage efficiencies of a solar air heater", *World Wide Journal of Multidisciplinary Research and Development*, Vol. 4, (2018), 121-128.
2. Jasim Mahmood, A., "Thermal evaluation of a double-pass unglazed solar air heater with perforated plate and wire mesh layers", *Sustainability*, Vol. 12, (2020), 1-15. <https://doi.org/10.3390/su12093619>.
3. Shiravi, A.H., Firoozzadeh, M. and Lotfi, M., "Experimental study on the effects of air blowing and irradiance intensity on the performance of photovoltaic modules, using Central Composite Design", *Energy*, Vol. 238, (2022), 121633.
4. Lakshmi, D.V.N., Muthukumar, P. and Nayak, P.K., "Experimental investigations on active solar dryers integrated with thermal storage for drying of black pepper", *Renewable Energy*, Vol. 167, (2021), 728-739. <https://doi.org/10.1016/j.renene.2020.11.144>.
5. Shafiee, M., Farbeh, A.M. and Firoozzadeh, M., "Experimental Study on Using Oil-Based Nanofluids in a Vacuumed Tube Solar Water Heater; Exergy Analysis", *International Journal of Ambient Energy*, (2022), 1-24. <https://doi.org/10.1080/01430750.2022.2073267>.
6. Sorgulu, F. and Dincer, I., "Design and analysis of a solar tower power plant integrated with thermal energy storage system for cogeneration" *International Journal of Energy Research*, Vol. 43, (2019), 6151-6160. <https://doi.org/10.1002/er.4233>.
7. Karimipour-Fard, P. and Beheshti, H., "Performance enhancement and environmental impact analysis of a solar chimney power plant: Twenty-four-hour simulation in climate condition of isfahan province, iran" *International Journal of Engineering, Transactions B: Applications*, Vol. 30, (2017), 1260-1269. doi: 10.5829/ije.2017.30.08b.20.
8. Kouhikamali, R. and Hassani, M., "The Possibility of using Flat Plate Solar Collector Based on the Best Calculated Tilt Angle in the City of Rasht as a Case Study", *International Journal of Engineering, Transactions B: Applications*, Vol. 27, No. 8, 2014, 1297-1306. <https://doi.org/10.5829/idosi.ije.2014.27.08b.16>.
9. Goel, V., Hans, V.S., Singh, S., Kumar, R., Pathak, S.K., Singla, M., Bhattacharyya, S., Almatrafi, E., Gill, R.S. and Saini, R.P., "A comprehensive study on the progressive development and applications of solar air heaters", *Solar Energy*, Vol. 229, (2021), 112-147. <https://doi.org/10.1016/j.solener.2021.07.040>.
10. Rayeni, A.D. and Nassab, S.A., "Effects of gas radiation on thermal performances of single and double flow plane solar heaters", *International Journal of Engineering, Transactions*

- C: Aspects** Vol. 33, No. 6, 2020, 1156-1166. <https://doi.org/10.5829/ije.2020.33.06c.14>.
11. Razak, A.A., Majid, Z.A.A., Azmi, W.H., Ruslan, M.H., Choobchian, S., Najafi, G. and Sopian, K., "Review on matrix thermal absorber designs for solar air collector", **Renewable and Sustainable Energy Reviews**, Vol. 64, (2016), 682-693. <https://doi.org/10.1016/j.rser.2016.06.015>.
  12. Salih, S.M., Jalil, J.M. and Najim, S.E., "Experimental and numerical analysis of double-pass solar air heater utilizing multiple capsules PCM", **Renewable Energy**, Vol. 143, (2019), 1053-1066. <https://doi.org/10.1016/j.renene.2019.05.050>.
  13. Kumar, A. and Subhash, K., "Effect of roughness and glass cover on solar air heater performance-A review", **International Research Journal of Advanced Engineering and Science**, Vol. 2, (2017), 46-58.
  14. Kumar, P.G., Balaji, K., Sakthivadivel, D., Vigneswaran, V.S., Meikandan, M. and Velraj, R., "Effect of using low-cost thermal insulation material in a solar air heating system with a shot blasted V- 14 corrugated absorber plate", **Thermal Science and Engineering Progress**, Vol. 14, (2019), 100403. <https://doi.org/10.1016/j.tsep.2019.100403>.
  15. Abdelkader, T.K., Zhang, Y., Gaballah, E.S., Wang, S., Wan, Q., Fan, Q., "Energy and exergy analysis of a flat-plate solar air heater coated with carbon nanotubes and cupric oxide nanoparticles embedded in black paint", **Journal of Cleaner Production**, Vol. 250, (2020), 1-11. <https://doi.org/10.1016/j.jclepro.2019.119501>.
  16. Das, B., Mondol, J.D., Debnath, S., Pugsley, A., Smyth, M. and Zacharopoulos, A., "Effect of the absorber surface roughness on the performance of a solar air collector: An experimental investigation", **Renewable Energy**, Vol. 152, (2020), 567-578. <https://doi.org/10.1016/j.renene.2020.01.056>.
  17. Jalil, J.M., Nothim, R.F. and Hameed, M.M., "Effect of Wavy Fins on Thermal Performance of Double Pass Solar Air Heater", **Engineering and Technology Journal**, Vol. 39, (2021), 1362-1368. <http://doi.org/10.30684/etj.v39i9.1775>.
  18. Sudhakar, P. and Cheralathan, M., "Thermal performance enhancement of solar air collector using a novel V-groove absorber plate with pin-fins for drying agricultural products: an experimental study", **Journal of Thermal Analysis and Calorimetry**, Vol. 140, (2020), 2397-2408. <https://doi.org/10.1007/s10973-019-08952-9>.
  19. Mesgarpour, M., Heydari, A. and Wongwises, S., "Geometry optimization of double pass solar air heater with helical flow path", **Solar Energy**, Vol. 213, (2021), 67-80. <https://doi.org/10.1016/j.solener.2020.11.015>.
  20. Jalil, J.M. and Ali, S.J., "Thermal Investigations of Double Pass Solar Air Heater with Two Types of Porous Media of Different Thermal Conductivity", **Engineering and Technology Journal**, Vol. 39, (2021), 79-88. <http://dx.doi.org/10.30684/etj.v39i1A.1704>.
  21. Sajawal, M., Rehman, T.U., Ali, H.M., Sajjad, U., Raza, A. and Bhatti, M.S., "Experimental thermal performance analysis of finned tube-phase change material based double pass solar air heater", **Case Studies in Thermal Engineering**, Vol. 15, (2019), 1-25. <https://doi.org/10.1016/j.csite.2019.100543>.
  22. Muthukumaran, J. and Senthil, R., "Experimental performance of a solar air heater using straight and spiral absorber tubes with thermal energy storage", **Journal of Energy Storage**, Vol. 45, (2022), 103796. <https://doi.org/10.1016/j.est.2021.103796>.
  23. Raju, G. and Kumar, M. M., "Experimental study on solar air heater with encapsulated phase change material on its absorber plate", **Energy Storage**, Vol. 3, (2021), 1-16. <https://doi.org/10.1002/est2.256>.
  24. Sudhakar, P. and Cheralathan, M., "Encapsulated PCM based double pass solar air heater: A comparative experimental study", **Chemical Engineering Communications**, Vol. 208, (2021), 788-800. <https://doi.org/10.1080/00986445.2019.1641701>.
  25. Abed, A.H., "Thermal storage efficiency enhancement for solar air heater using a combined SHSm and PCM cylindrical capsules system: experimental investigation", **Engineering and Technology Journal**, Vol. 34, (2016), 999-1011.
  26. Kumar, K., Kaushik, S. and Bisht, V.S., "CFD analysis on solar air heater with artificial roughened broken curved ribs", **International Journal of Scientific & Engineering Research**, Vol. 8, (2017), 264-275.
  27. Yadav, A. S. and Bhagoria, J. L., "Modeling and simulation of turbulent flows through a solar air heater having square-sectioned transverse rib roughness on the absorber plate", **The Scientific World Journal**, Vol. 2013, (2013), 1-12. <https://doi.org/10.1155/2013/827131>.
  28. Sharol, A. F., Razak, A. A., Majid, Z. A., Azmi, M. A. and Tarmizi, M. A., "Evaluation on the performance of cross-matrix absorber double-pass solar air heater (CMA-DPSAH) with and without thermal energy storage material", **Journal of Advanced Research in Fluid Mechanics and Thermal Sciences**, Vol. 70, No. 2, (2020), 37-49. <https://doi.org/10.37934/arfmts.70.2.3749>.
  29. Sharol, A. F., Abdul Razak, A., Abdul Majid, Z. A. and Fudholi, A., "Experimental study on performance of square tube absorber with phase change material", **International Journal of Energy Research**, Vol. 44, No. 2, (2020), 1-12. <https://doi.org/10.1002/er.4971>.
  30. Hussien, S.Q. and Farhan, A. A., "The effect of metal foam fins on the thermo-hydraulic performance of a solar air heater", **International Journal of Scientific & Engineering Research**, Vol. 9, No. 2, (2019), 840-847.
  31. Hassan, H., Abo-Elfadl S. and El-Dosoky MF., "An experimental investigation of the performance of new design of solar air heater (tubular)", **Renewable Energy**, Vol. 151, (2020), 1055-1066. <https://doi.org/10.1016/j.renene.2019.11.112>.
  32. Bergman, T.L., and Incropera, F.P., "Fundamentals of heat and mass transfer", John Wiley & Sons, (2011).
  33. Salih, S.M., Jalil, J.M. and Najim, S.E., "Double-Pass Solar air Heater (DP-SAH) utilizing Latent Thermal Energy Storage (LTES)" in 2nd International Conference on Sustainable Engineering Techniques, Baghdad, Iraq, (2019), 32001-32010, <https://doi:10.1088/1757-899X/518/3/032038>.
  34. Mohammed, A. "Study of Double Pass Solar Air Heater Integrated with A Thermal Storage Material", PhD thesis, University of Technology, Baghdad, Iraq, (2017).

---

### Persian Abstract

---

**چکیده**

مشکل تابش خورشیدی متناوب می‌تواند به طور قابل توجهی بر عملکرد حرارتی بخاری‌های هوای خورشیدی (SAHs) تأثیر بگذارد. راه حل کارآمد برای این مشکل استفاده از ذخیره سازی حرارتی برای ذخیره انرژی حرارتی و استفاده مجدد از آن در ساعات غیر آفتابی است. مطالعه حاضر عملکرد حرارتی دو پیکربندی از گرمکن هوای خورشیدی دو گذری جريان مقابله تحليل کرد. پیکربندی اول شامل پک جاذب خورشیدی صفحه تخت بود، در حالی که پیکربندی دوم شامل کپسول‌های لوله‌ای است که با آب به عنوان یک ماده ذخیره حرارتی معقول پر می‌شود. کپسول‌های لوله‌ای به صورت طولی و موازی جهت جريان هوا نصب شده‌اند. اين مطالعه شامل بخش‌های عددی و تجربی بود. نتایج افزایش قابل توجهی را در تولید انرژی مفید هنگام استفاده از کپسول‌های لوله‌ای نشان داد. علاوه بر اين، SAH با کپسول‌های لوله‌ای به دليل وجود مواد ذخیره‌سازی حرارتی درون کپسول‌ها، می‌تواند برای مدت طولانی‌تری انرژی مفید تولید کند. مشخص شده است که کل انرژی مفید در مورد کپسول‌های لوله‌ای در حدود ۴۲۹۵.۳، ۴۰۵۸، ۴۲۶۴، ۴۵۸۴، ۴۶۹۳ و ۴۴۲۶ (W) با سرعت جريان جرمی ۰.۰۳، ۰.۰۲۵، ۰.۰۲، ۰.۰۱۵، ۰.۰۱ و ۰.۰۰۱ کیلوگرم بر ثانیه است. با افزایش ۰.۳۸.۳، ۰.۵۱.۲، ۰.۷۴.۸، ۰.۵۹.۴ و ۰.۸۹.۶ درصد نسبت به صفحه تخت. علاوه بر اين، متوسط راندمان ترمohیدروليک در مورد کپسول‌های لوله‌ای بيشتر از مقاديری است که در صفحه تخت در حدود ۰.۹.۳ و ۰.۱۵، ۰.۱۹.۶، ۰.۲۸.۲ درصد در نرخ جريان جرمی ۰.۰۲۵، ۰.۰۱۵، ۰.۰۱ و ۰.۰۰۱ کیلوگرم بر ثانیه است.

---